Technical Report

TR-13-09

Hydrogen in oxygen-free, phosphorus-doped copper: charging techniques, hydrogen contents and modelling of hydrogen diffusion and depth profile

Åsa Martinsson, Swerea KIMAB

Rolf Sandström
Swerea KIMAB and Materials Science and Engineering, KTH

Christina Lilja, Svensk Kärnbränslehantering AB

January 2013

Svensk Kärnbränslehantering AB
Swedish Nuclear Fuel
and Waste Management Co

Box 250, SE-101 24 Stockholm
Phone +46 8 459 84 00

ISSN 1404-0344
SKB TR-13-09
ID 1375899

Hydrogen in oxygen-free, phosphorus-doped copper: charging techniques, hydrogen contents and modelling of hydrogen diffusion and depth profile

Åsa Martinsson*, Swerea KIMAB

Rolf Sandström
Swerea KIMAB and Materials Science and Engineering, KTH

Christina Lilja, Svensk Kärnbränslehantering AB

January 2013

*Now at Sandvik Materials Technology

Keywords: Oxygen-free copper, Cathodic charging, Thermal charging, Hydrogen profile, Grain size, Bubble nucleation.

Abstract

In Sweden spent nuclear fuel is planned to be disposed of by encapsulating in cast iron inserts protected by a copper shell. The copper can be exposed to hydrogen released during corrosion processes in the inserts. If the hydrogen is taken up by the copper, it could lead to hydrogen embrittlement. Specimens from oxygen-free copper have been hydrogen charged using two different methods. The purpose was to investigate how hydrogen could be introduced into copper in a controlled way. The thermal charging method resulted in a reduction of the initial hydrogen content. After electrochemical charging of cylindrical specimens, the measured hydrogen content was 2.6 wt. ppm which should compared with 0.6 wt. ppm before charging. The retained hydrogen after two weeks was reduced by nearly 40%.

Recently the paper “Hydrogen depth profile in phosphorus-doped, oxygen-free copper after cathodic charging” (Martinsson and Sandström, 2012) has been published. The paper describes experimental results for bulk specimens as well as presenting a model. Almost all the hydrogen is found to be located less than 100 μm from the surface. This model is used to interpret the experimental results on foils in the present report. Since the model is fully based on fundamental equations, it can be used to analyse what happens in new situations. In this report the effect of the charging intensity, the grain size, the critical nucleus size for hydrogen bubble formation as well as the charging time are analysed.

Contents

1 Background

Spent nuclear fuel in Sweden is planned to be disposed of by encapsulation in cast iron inserts placed inside copper canisters. The cast iron is load bearing and the copper shell gives protection against corrosion in the geological repository. Inherent in the encapsulation process is the risk of water inclusion in the canister before sealing which cannot totally be ruled out. One scenario is that up to 600 g of water can be trapped inside the fuel elements in the canister during encapsulation (SKB 2006). The water can then be consumed by corrosion processes and hydrogen released. Hydrogen is also released from corrosion of iron if there is a hole in the copper shell and groundwater is intruding. The risk for hydrogen uptake needs therefore to be studied.

Hydrogen embrittlement is a well-known phenomenon. Examples of hydrogen induced damage include formation of internal voids and cracks, loss of ductility, and high temperature hydrogen attack.

Although extensive research work has been devoted to hydrogen embrittlement in various metals and alloys, see a summary in Dayal and Parvathavarthini (2003), this phenomenon is at present not completely understood. Studies of the effect of hydrogen on mechanical properties of copper are even more limited. In a study, Nieh and Nix (1980) first introduced oxygen in pure copper by heat treating at 800°C and after that heat treated the copper in pure hydrogen at 600°C to get significant amounts of hydrogen into the material. Examining the mechanism governing intergranular cavity growth in this material, they reported that almost all of the cavities are formed at grain boundaries, primarily because oxygen strongly segregates to grain boundaries. As a consequence, creep strength and ductility were markedly reduced.

The classical form of hydrogen embrittlement of copper has been attributed to formation of voids generated by reaction between diffusing hydrogen and cuprous oxide inclusions (Caskey et al. 1975). Oxygen is nearly insoluble in copper, e.g. in electrolytic tough-pitch copper, and forms interdendritic and intergranular Cu_2O when the copper is manufactured. For many applications the oxygen is an insignificant impurity. However, when copper is heated to a temperature above approximately 400°C, for instance during welding or heat treatment, the hydrogen can diffuse into the copper and react with the internally dispersed Cu_2O to form steam according to the chemical reaction:

$Cu_2O + H_2(\text{dissolved in Cu}) \rightarrow 2Cu + H_2O(g)$

The large water molecules formed by the reaction do not diffuse readily in copper and develop into internal voids, particularly at grain boundaries, which makes the copper brittle.

To avoid the classical form of hydrogen embrittlement oxygen free copper is used, Cu-OF and Cu-OFP. However, it is well documented that hydrogen in the absence of oxygen can also induce embrittlement due to a modified dislocation structure or at larger contents hydrogen porosity (Nakahara 1988). Only this type will be analysed in the present report. Wampler et al. (1976) found that in pure copper, hydrogen charged to 65 and 70 at. ppm, hydrogen precipitated as bubbles between 0 and 50°C. The formation of bubbles was accompanied by the emission of dislocation loops around the bubbles.

Observed effects of hydrogen on mechanical properties include increased tensile strength and hardness, but reduced ductility. The equilibrium solubility of hydrogen in copper increases with increasing temperature (Nakahara and Okinaka 1988). According to the experimental data obtained by McLellan (1973), the amount of hydrogen θ in copper in equilibrium with 1 atm. hydrogen gas can be expressed as

$$\ln\theta = -\frac{6.62\times10^3}{T} - 4.48 \qquad \text{Eq (1)}$$

where T is the temperature in Kelvin and θ is expressed as 10^6 at. ppm. Using Eq (1), one obtains about 3×10^{-6} at. ppm H at 25°C and about 40 at. ppm H at 900°C (Nakahara and Okinaka 1988). This means that copper absorbs almost no hydrogen at room temperature but the equilibrium

solubility rises by a factor of 107 at 900°C. To get for example 6 at. ppm hydrogen into copper by heat treating in pure hydrogen, it requires a temperature of 600°C. This is also in agreement with the observations of Nieh and Nix (1980).

Introduction of hydrogen into copper is usually conducted by one of the following three processes; namely *i)* thermal charging, *ii)* cathodic charging and *iii)* electroless copper plating. A detailed description of these three processes is given in Nakahara and Okinaka (1988). Actually, both thermal charging (Pan 1986, Pan and Byrne 1985, Hoelzel 2004) and cathodic charging (Nakahara and Okinaka 1989, Panagopoulos and Zacharopoulos 1994, Pisarek and Janik-Czachor 2006, Au 2003, Dull and Raymond 1974) have been applied to introduce hydrogen in copper and steels. The driving force for the thermal charging is hydrogen pressure gradient. This method is a traditional approach and requires high temperature and high hydrogen pressure and usually takes long time. Based on data given in McLellan (1973), pure hydrogen gas heat treatment at 480 and 600°C is needed to introduce 2 and 6 at. ppm, respectively at 1 atm. The driving force for cathodic charging is the electrochemical potential. Since migration of hydrogen ions is faster than diffusion of hydrogen atoms in a thermal hydrogen charge, the cathodic charging offers convenient means for injecting atomic hydrogen into copper at ambient temperatures. It can build up higher levels of hydrogen in a short period. The difficulty lies in knowing the exact hydrogen content that has been introduced. In the literature, the electroless copper plating method has only been used on copper films, which is why we have chosen not to use it in this study.

Established techniques are available for measurement of the hydrogen content. The two most accurate ones are melt extraction and controlled outgassing. However, if the position of the hydrogen in the microstructure is of interest or if it is important to distinguish between hydrogen in atom and molecule form, the situation is more complicated. It has been shown that secondary ion mass spectrometry (SIMS) is a sensitive analysis method for hydrogen. Hydrogen desorption from copper during ion bombardment has been measured and analysed (Nagai et al. 1996). It shows that the amount of hydrogen can be detected locally, e.g. at grain boundaries.

The aims of this study are firstly to investigate if hydrogen can be introduced in copper in a controlled way and then to use a previously published model to describe how charging and micro-structure influence the hydrogen content.

2 Material

The material tested in this study is a pure, oxygen-free copper doped with phosphorus (Cu-OFP) provided by Svensk Kärnbränslehantering AB (Swedish Nuclear Fuel and Waste Management Company, SKB). The specimens were cut out from a forged canister lid with the designation TX104. A more detailed description of the material and its chemical composition is found in Martinsson and Sandström (2012).

Two different types of specimens were used for hydrogen charging. The cylindrical specimen had a diameter of 5 mm and a length of 8 mm. These dimensions are the same as a section from the gauge length of the intended creep specimen.

Specimens were also produced in the form of foils with varying thickness. First, two specimens in the size 10×10 mm were cut out from a 0.1 mm commercial foil. This material was not provided by SKB, and the material condition of this material has not been established. These foils were initially annealed at 800°C in order to remove internal stresses. Second, foils were produced from the copper lid TX104. Sheets of 0.7 mm thickness were manufactured by spark machining and then ground with SiC paper (down to mesh 1200) to the final thickness. Sheet of 2 mm thickness was cut out from the same lid and cold rolled to 0.25 mm thickness. All specimens, foils and bars, were electropolished (in 50% ortophosphoric acid for 5–10 s at a voltage of 2V) before hydrogen charging in order to remove oxides and to ensure a clean surface.

3 Experimental

3.1 Thermal charging

To investigate the influence of the thermal charging on the grain size, an initial heat treatment was performed. Specimens were heat treated for 1 or 10 hours at 675 and 750°C. The average grain size was measured both in sections parallel and perpendicular to the axial direction of the specimens.

The thermal charging was carried out in a tube furnace. The specimens were placed on a wire tray inside the furnace to allow as much surface as possible to be in contact with the gas. A thermocouple was placed inside the furnace close to the tray for temperature control. The furnace was vacuum pumped before the hydrogen gas flow was started. The flow of pure hydrogen gas (industrial quality, 99.95%) was kept constant during the heating of the furnace up to the charging temperature and also during the charging period. A small external pressure was applied to maintain the flow of the gas. When the charging was finished the hydrogen flow was replaced with argon for a few minutes before the furnace was opened. The specimens were quenched in H_2O and then stored in liquid nitrogen until the moment of analysis. Five specimens in each series were charged simultaneously in the furnace.

3.2 Electrochemical charging

One advantage of electrochemical charging is that it can be carried out at room temperature. Figure 3-1 shows the simple experimental set-up which includes a source of power supply with constant current mode, a platinum counter electrode and an electrolyte. Two specimens were charged simultaneously in order to investigate the distribution of the hydrogen content and the repetitiveness of the charging. The specimens were connected to the negative pole on the power supply by a copper wire twirled around the specimen or soldered to the end of the cylinders. The platinum counter electrode was connected to the positive pole. The specimens and the counter electrode were placed in a beaker which was filled with an electrolyte to enable an electrical contact between the poles. A constant current density was applied to create a difference in electrochemical potential between the specimens and the counter electrode. The subsequent reaction at the counter electrode is

$$2\ H_2O \rightarrow O_2\ (g) + 4\ H^+ + 4\ e^- \qquad \text{Eq (2)}$$

where H^+ and e^- are released through decomposition of water. The rate of the process can be affected by the choice of electrolyte. H_2SO_4 is a more aggressive electrolyte than Na_2SO_4 and will therefore have a greater influence on the charging. The released components are then included in the following reactions taking place at the surface of the specimen:

$$2\ H^+ + 2\ e^- \rightarrow 2\ H_{ads} \qquad \text{Eq (3)}$$

$$2\ H_{ads} \rightarrow H_2\ (g) \qquad \text{Eq (4)}$$

$$H_{ads} \rightarrow H_{abs} \qquad \text{Eq (5)}$$

The atomic hydrogen produced at the surface of the specimen will either form hydrogen gas and evaporate or be absorbed into the bulk of the specimen. The addition of arsenic to the electrolyte will impede the reaction indicated by Eq (4) and thereby facilitate the hydrogen charging.

Electrochemical charging is a time consuming method. To investigate the solubility limit of hydrogen in copper in a reasonably short time foils were chosen as initial charging specimens. Thereafter the study continued with the thicker, cylindrical specimens.

The electrolyte used in this study was 10% H_2SO_4 + 60 mg/l As_2O_3. The applied current densities were 5.5 and 10 mA/cm^2. The charging times were 24, 145 and 504 h. The charging parameters were altered with the purpose of increasing the hydrogen content in the specimens and make the process more efficient. The hydrogen content of the specimens was analysed immediately after charging. The same analysing method as for thermally charged specimens was used.

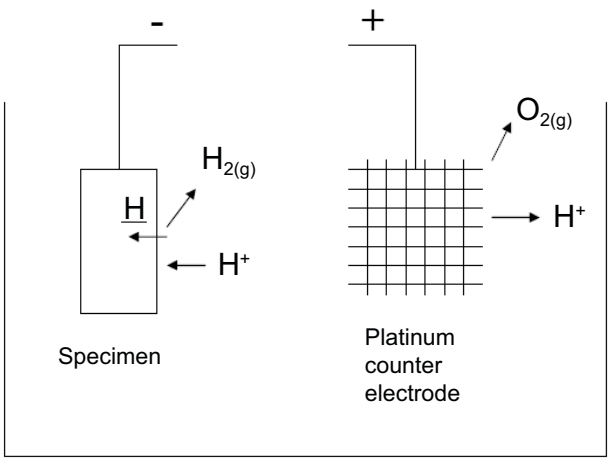

Figure 3-1. *Schematic drawing of the experimental set-up for electrochemical charging.*

3.3 Hydrogen analysis

The analysis of hydrogen content was performed in a Leco Rhen 602 hydrogen determinator. The specimens were melted in argon atmosphere whereupon the hydrogen in the sample was released in the form of gas. The hydrogen content was determined by measuring the heat conductivity of the gas mix during the analysis process. This analysis method was used for both thermal and electrochemical charging.

4 Experimental results

4.1 Grain coarsening by thermal charging

Figure 4-1 shows the average grain size in the copper specimens after heat treatment corresponding to thermal charging parameters. The grain size in the as-received material was < 200 µm in both axial and transverse sections. During heat treatment at 675°C grain growth occurred and the average grain size was found to be within 220 and 370 µm. The time had little influence on the growth along the axial section. However the grain growth was larger at the transverse section after the longer charging time. The effect of the heat treatment at 750°C was significant. The difference in grain size between the two directions is larger, especially after 10 h heating. However, the most important result is that the grain size in the transverse section exceeds 1,380 µm after thermal charging at 750°C. The maximum average grain size allowed in the material is 360 µm (Raiko et al. 2010). Thermal charging at 750°C and above was therefore not performed.

4.2 Thermal charging

The hydrogen content in the copper after thermal charging is presented in Table 4-1. The charging was made on cylindrical specimens only. Charging was not performed at 750°C due to the measured grain growth. Instead charging was performed at 675 and 600°C to reduce the thermal influence on the microstructure. The variation of hydrogen content on the different samples is minor, see Table 4-1. Due to intermittent problems with the analysis equipment not all charged specimens were analysed and can therefore not be included in the results. The charging was performed for 1 hour at 675°C and for 10 hours at 600°C. The average hydrogen content in the as-received material was 0.68 weight ppm (wt. ppm), see Table 4-1. After 1 hour of thermal charging at the higher temperature, the hydrogen content is more or less unaffected. After 10 hours at the lower temperature the hydrogen content in the specimens is reduced by almost 50%.

Table 4-1. Results from thermal charging.

Material	Temperature, °C	Time, h	Average H content, wt. ppm	H content, wt. ppm
Cu ref	–	–	0.68±0.12	0.76 0.60
Cu	675	1	0.72±0.11	0.82 0.73 0.76 0.55
Cu	600	10	0.36±0.07	0.33 0.44 0.30

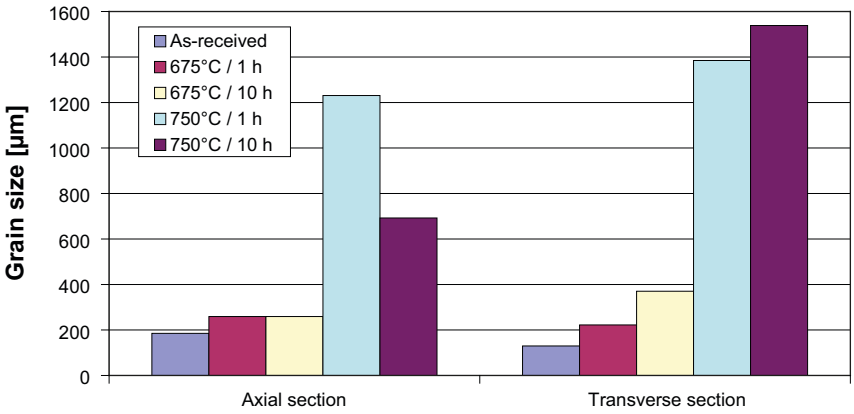

Figure 4-1. *The average grain size after heat treatment of Cu-OFP.*

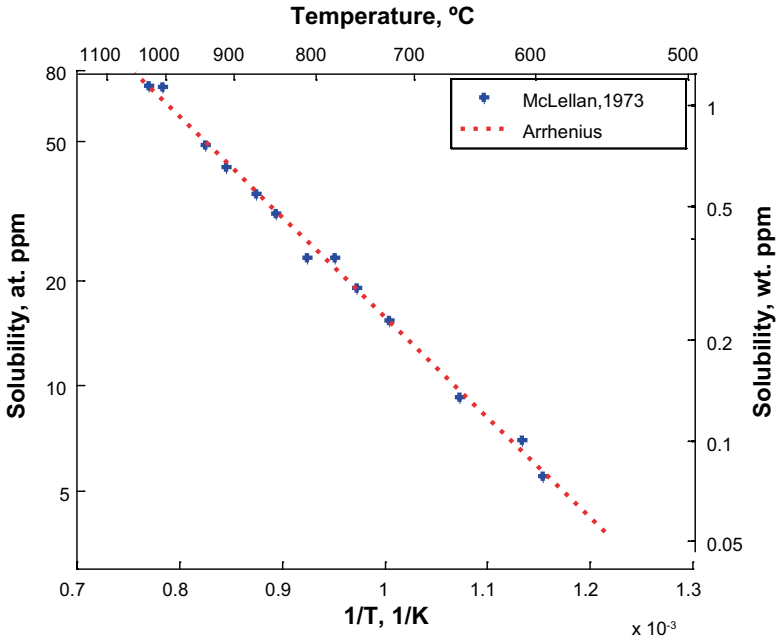

Figure 4-2. *Solubility of hydrogen in copper in at. ppm (left scale) or wt. ppm (right scale) as a function of inverse absolute temperature. The experimental data is from McLellan (1973). The model is the Arrhenius expression in Eq (6).*

Data for hydrogen solubility in copper from McLellan (1973) is shown in Figure 4-2 .The following expression that has been fitted to the data is also shown

$$H_{sol} = 1.152 \times 10^4 e^{-\frac{54850}{RT}} \quad \text{at. ppm} \qquad \text{Eq (6)}$$

where R and T are the gas constant and absolute temperature, respectively. We can see that the fit in Eq (6) is an adequate representation of the experimental data. From Figure 4-2 it is evident that the hydrogen solubility at the investigated temperatures is 0.1 to 0.2 wt. ppm which is lower than the original reference value of about 0.7 wt. ppm. There is consequently no surprise that no hydrogen charging has taken place at 600 and 675°C. At 600°C a clear reduction of the hydrogen content is also observed. From Figure 4-2 it can be seen that a temperature exceeding 900°C would be required to raise the hydrogen content in copper in an atmosphere of 1 atm. hydrogen. As discussed above such a high temperature is not practical to use since it would lead to a significant change in the microstructure.

4.3 Electrochemical charging

The results from electrochemical charging of bars are found in Table 4-2 and Figure 4-3. Two series of cylindrical specimens were electrochemically charged at a current density of 5.5 and 10 mA/cm^2, respectively. The electrical contact between the specimen and the wire was during the latter charging not optimal due to deposition formed on the surface of the specimen. The test was repeated with the wire soldered to the cylinder instead of twirled around it. The repeated test gave an average hydrogen content of 2.91 wt. ppm for 10 mA/cm^2 compared to 1.44 wt. ppm for 5.5 mA/cm^2, both charged during 24 h, and 0.58 wt. ppm for as-received material.

The first long-term charging at 10 mA/cm^2 was interrupted nearly 16 days after the test was launched because of a broken wire. Nevertheless the specimens were analysed directly after the discovery, which was maximum 2 days after the failure. The hydrogen content was higher than after 24 h, but significantly lower in the specimen in which the wire broke. To examine how strongly the hydrogen is bound to the copper a new test was started. Two series with identical charging parameters were launched. The deposition was removed from all specimens by mechanical grinding. One series was analysed directly after the 504 h long charging period was finished. The other series was analysed 2 weeks later, after being stored in dry air at room temperature for the whole time. The average hydrogen content measured directly after the charging was 2.56 wt. ppm while the hydrogen value had diminished to 1.50 wt. ppm after 2 weeks at room temperature. Unfortunately the variation of the hydrogen values obtained directly after charging was high.

Table 4-2. Results from electrochemical charging of bars.

Material	Current density mA/cm^2	Time h	Average H content wt. ppm	H content wt. ppm	Comments
Cu cyl. ref	–	–	0.58 ± 0.03	0.55 0.63 0.57 0.61 0.59 0.55	
Cu cyl.	5.5	24	1.44 ± 0.21	1.59 1.29	
		145	2.02 ± 0.81	1.45 2.59	
	10.0	24	0.92 ± 0.12	0.84 1.01	a)
			2.91 ± 0.36	2.66 3.16	b)
		15–16 days	–	2.83 3.58	b), c) b), d)
		504	2.56 ± 1.2	3.4 1.71	b)
			1.50 ± 0.21	1.64 1.35	b), e)

a) Poor electrical contact, experiment repeated.

b) Wire soldered to the specimen.

c) Wire broken after 15–16 days.

d) Analysed directly after interrupted charging.

e) 2 weeks at room temperature before analysis.

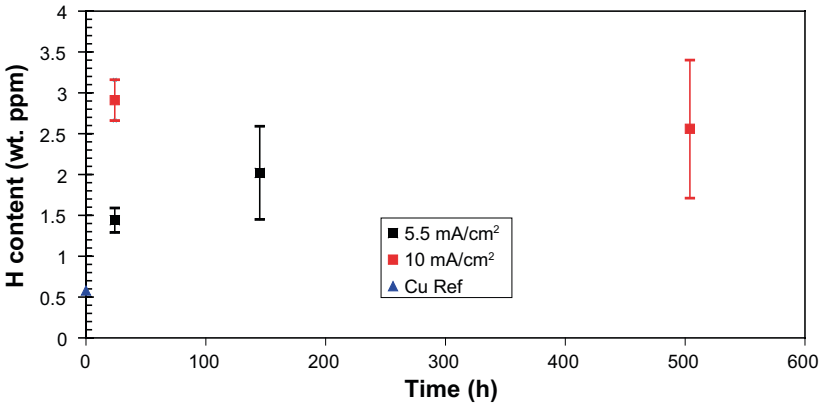

Figure 4-3. Hydrogen content versus charging time at given electrochemical charging conditions for cylindrical specimens. The lines indicate the max and min values while the averages are shown as squares.

The results from electrochemical charging of foils are found in Table 4-3. The first part of the experiment of charging and analysing foils was made on a commercial 0.1 mm thin foil. Ten days of charging was expected to be enough to reach the solubility limit. Only two specimens were hydrogen charged, and resulted in a vast difference in hydrogen content, and a high hydrogen content for one of the specimens compared to the uncharged copper foils.

The second part was initiated to establish if the copper alloy used in the canisters was to behave in a similar way. Table 4-3 shows that the hydrogen content in the reference foils was approximately 4 wt. ppm, which is almost 6 times higher than the hydrogen content measured in the reference bars taken from the same lid. It seems likely that hydrogen was introduced into foils during the spark machining.

As-received copper foils were hydrogen charged for 5 hours, 10 hours and 7 days, two specimens at each charging time. The specimens charged at 5 and 10 hours had approximately the same foil thickness, while the 7-days-charged specimens were thinner. The highest content by far was obtained after 10 hours of charging. A joint behaviour of each as-received pair is that there is a great difference in hydrogen content between the two specimens. Two cold-rolled specimens were hydrogen charged for 7 days and analysed, resulting in a similar hydrogen content and distribution as the as-received material charged for the same time.

Table 4-3. Results from electrochemical charging of foils.

Material	Thickness [mm]	Current density [mA/cm^2]	Time	Average H content [wt. ppm]	H content [wt. ppm]	Comments
Commercial Cu foil ref	0.1	–	–	1.27 ± 0.27	1.46	a), b)
					1.08	
Commercial Cu foil	0.1	9.9	10 days	154 ± 130	62.48	
					246.3	
As-received Cu foil ref	0.39	–	–	3.98 ± 2.27	2.10	b)
	0.38	–	–		1.97	
	0.3	–	–		6.34	
	0.3	–	–		5.49	
Cold-rolled Cu foil	0.26	10	7 days	30.3 ± 20.3	44.70	b)
	0.25				15.98	
As-received Cu foil	0.15	10	7 days	30.4 ± 20.6	44.99	b)
	0.25				15.82	
	0.3		5 hours	11.8 ± 5.61	7.83	
	0.37				15.76	
	0.3		10 hours	238 ± 118	321.88	
	0.37				154.57	

a) Annealed before charging.

b) Electropolished before charging.

5 Discussion of experimental results

Hydrogen introduced in a material can be locked in the parent metal when in molecular form or be more mobile when in atomic form. Wampler et al. (1976) studied the mobility of the retained hydrogen atoms in thermally charged single crystal copper using resistivity measurements. They found that the hydrogen becomes mobile above –130°C and precipitates into bubbles above 0°C. The bubbles are surrounded by dislocation tangles. In polycrystalline copper the bubbles preferentially form at grain boundaries.

Thermal hydrogen charging has been proven to be a useful method to introduce and retain hydrogen. This is why the thermal charging method was chosen in this study. The charging was performed with the same parameters as in Wampler et al. (1976) except for the external pressure that was not possible to achieve in the accessible equipment. The results show that the thermal charging does not render higher hydrogen content in the copper. Instead the procedure is transformed into an outgassing method, which is consistent with the low hydrogen solubility in copper. It is believed that the driving force of this process is the hydrogen activity gradient (Kennedy et al. 1993). Wampler et al. managed to thermally charge copper without external pressure, but the temperature they used was far above our limit at 675°C, which was fixed to avoid grain growth. The thermal charging was therefore disregarded as a suitable charging method.

There are two ways that the hydrogen from the corrosion inside the insert can reach the canister wall. Hydrogen can enter the cast iron and diffuse through the insert or a hole through the insert can have been formed. This is expected to create a modest hydrogen pressure at the inside of the canister. From the experimental results on thermal charging, it can be concluded that this will not give rise to any uptake of hydrogen in the copper due to the low temperature of the canister (< 100°C).

Results of how hydrogen affects microstructure and properties of copper after electrochemical charging have been presented in several publications (Nakahara and Okinaka 1988, 1989, Panagopoulos and Zacharopoulos 1994, Pisarek and Janik-Czachor 2006). However, none of the authors have specified the amount of hydrogen introduced during charging. A parallel study on hydrogen effects in cast iron (Martinsson et al. 2009) using the same charging equipments as in this study showed that the electrochemical charging method gave a higher hydrogen content than what was obtained by thermal charging. Another important advantage is that grain growth is avoided, which is of great significance for material intended for creep testing.

Several charging procedures were carried out with cylindrical specimens to optimise the parameters and the final hydrogen content. The set-up was tested and the functionality of the electrolyte confirmed before the optimal current density was determined. Subsequently the time was increased from 24 h to 504 h. The hydrogen content in the double-sample was measured after 24 h charging, which resulted in hydrogen amounts 3.6 and 4.4 times higher than the reference specimens. After 504 h the hydrogen content in the double-sample was 4.9 and 1.9 times higher than the references. The large spread of hydrogen content in some of the initial tests was most likely caused by poor electrical contact between wire and specimen. In the 504 hours test the wire was soldered to the specimens, which should secure that sufficient electrical contact was always maintained. The reason why one specimen contained 3.40 wt. ppm after charging and the content of hydrogen in the other one was as low as 1.71 wt. ppm is not clear. Both specimens have been charged in the same electrolyte-filled beaker with the same applied current. Based on the results after 24 h charging, the specimen with the lower content must be considered to be the divergent specimen. The true value is therefore assumed to be closer to 3.40 wt. ppm, which still is a relatively small amount. The increase of charging time from 24 to 504 h was not reflected in the measurement of the hydrogen content. Instead, the results indicate that the obtained values are close to the solubility limit. Therefore no other charging times were investigated.

One reason for the low hydrogen content after charging is the use of oxygen-free copper. The oxygen is preferentially found at the grain boundaries (Nieh and Nix 1980). If the oxygen content is not reduced, it can react with the hydrogen atoms and form water molecules, which will increase the amount of retained hydrogen in the copper. A reduction of oxygen decreases the possibilities for hydrogen to accumulate in the copper. For the same reasons, the content of other foreign elements have been minimized in order to avoid inclusions or contaminations that will attract the hydrogen.

Creep testing of hydrogen charged specimens requires not only an enhanced content immediately after the charging, but also a significant amount of retained hydrogen throughout the creep testing period. To get an indication of the mobility of hydrogen in Cu-OFP a double-sample was charged during 504 h. The analysis of the hydrogen content was performed 2 weeks after the charging was finished, during which time the specimens had been stored in dry air at room temperature. During these two weeks, the amount of hydrogen had been reduced by about 40% compared to the specimens measured directly after charging.

The hydrogen content immediately after charging is low and is further reduced as early as after two weeks at room temperature. The hydrogen content in the copper will decrease more rapidly at higher temperatures. The temperature in the copper canister will be close to 100°C initially and then decrease slowly during thousands of years. Based on the test results produced in this study, the outgassing will be so extensive that creep testing is purposeless under these conditions.

One of the most important electrochemical charging parameters is the time. In order to investigate how fast the solubility limit can be reached in a sample, a thin specimen of a commercial foil was chosen to minimize the time required for the experiment. Ten days was considered to be enough to reach the solubility limit. The hydrogen content of the annealed foil was analysed and determined to be 1.27 wt. ppm, which is twice as much as in the Cu-OFP reference material. After charging, the hydrogen content in the foil was measured to 62.48 wt. ppm in one of the double-samples and 246.3 wt. ppm in the other, which is an unacceptably large difference. Its origin is not known.

Due to the different hydrogen content before charging in the annealed foils compared to the lid material, the unknown material condition of the foils and the high hydrogen content after charging, new series of testing was initiated with copper foils produced from the canister lid. That the as-received foils from the canister lid resulted in an almost 6 times higher hydrogen content than the bars, with the only difference being the dimensions of the specimens, was an indication that the choice of method for charging can have an influence on the results. That the highest hydrogen content was not obtained after 7 days of charging, but after 10 hours, and in addition in thicker specimens, was an unexpected result. The hydrogen atoms introduced into the copper transports by diffusion, and with increased charging time the hydrogen content would consequently increase with the time. Together with the large inconsistency between the specimens charged with the same set of parameters, it was clear that it was not possible to hydrogen charge copper foils with this method and expect reliable and reproducible results. It is possible that surface oxides that form on the copper at room temperature and other surface contaminations can contribute to the inconsistency of the results. Due to the higher specific surface area of the foils compared to the bars, the influence of the surface on the analysis results will be significant.

6 Analysis of hydrogen bubble nucleation and growth in copper

In the experimental work presented above it is quite clear that the surface of the specimens plays an important role for the uptake of hydrogen. The mechanisms for this effect are the topic of a recent paper "Hydrogen depth profile in phosphorus-doped, oxygen-free copper after cathodic charging" (Martinsson and Sandström 2012). The paper describes new experimental techniques for determining the penetration of the hydrogen charging in bulk specimens. A three-step profile method was developed and was used instead in combination with Glow Discharged Optical Emission Spectroscopy (GDOES) measurements (Martinsson and Sandström 2012). A model was also presented that could describe the experimental results. The experiments in the paper were based on maximum cathodic charging. The results are, however, of interest to apply to conditions with more modest charging, for example during corrosion. Since the model is entirely based on fundamental equations, it can be used to analyse what happens in new situations. In this report the effect of the charging intensity, the grain size, the critical nucleus size for hydrogen bubble formation as well as the charging time is analysed.

6.1 Basic assumptions in the model

This section gives a brief description of the model in Martinsson and Sandström (2012) (referred to as the *paper* whereas this text is called the *report*).

The transport of hydrogen into the material is controlled by diffusion of hydrogen atoms, which satisfies the diffusion equation

$$\frac{dc_H}{dt} = D\frac{d^2c_H}{dy^2} \qquad \text{Eq (7)}$$

where c_H is the concentration of atomic hydrogen in solid solution, t the time, D the diffusion constant for hydrogen and y the distance from the surface. Hydrogen flows into bubbles, where the hydrogen transforms to molecules. The diffusion back to the matrix from bubbles is not considered due to low concentration of atomic hydrogen in the bubbles. The flux J_H of hydrogen to a bubble can be expressed as

$$J_H = D\nabla c_H = D\frac{c_H}{r} \qquad \text{Eq (8)}$$

where r is the bubble radius. Due to inflow the bubbles grow in size

$$\frac{dr}{dt} = \frac{D}{\rho_H}\frac{c_H}{r} \qquad \text{Eq (9)}$$

ρ_H is the density of hydrogen in the bubbles [kg/m^3]. The bubble must be larger than a critical radius r_{crit} to be able to grow

$$r_{crit} = \frac{2\gamma}{p} \qquad \text{Eq (10)}$$

where γ is the surface energy of the bubble and p the hydrogen pressure in it. The number of bubbles per unit volume n_V, is analysed below. With the aid of stereology, n_V can be related to the number of bubbles per unit area n_A. This requires that the bubbles are approximately randomly distributed

$$n_A = 2rn_V \qquad \text{Eq (11)}$$

Due to the flux into the bubbles, there is a change of concentration c_H of atomic hydrogen in solution, cf. Eq (9)

$$\frac{dc_H}{dt} = -4\pi r^2 n_V D \frac{c_H}{r} \qquad \text{Eq (12)}$$

By adding this contribution to (7) and applying (11) gives the resulting diffusion equation

$$\frac{dc_H}{dt} = D\frac{d^2 c_H}{dy^2} - 2\pi n_A D c_H \qquad \text{Eq (13)}$$

Eqs (9) and (13) represent a system for bubble radii and hydrogen content. This system can be solved numerically. The solution depends on a number of parameters. Two of these namely the diffusion constant D and the surface energy γ have well established values and do not vary with charging conditions or the microstructure. At room temperature D is equal to 2.2×10^{-14} m/s^2 (Ishikawa and McLellan 1985). The surface energy γ takes the value 2.0 J/m^2 (Vitos et al. 1998). The number of bubble nuclei per unit area n_A depends on the grain size d. The hydrogen pressure p in the bubbles affects the size of their nuclei r_{crit}, Eq (10). The inflow of hydrogen through the surface J can only be assessed indirectly. r_{crit} and J are start values (boundary conditions) when integrating the system of equations. In the next few sections the consequences of variation of the parameters d, r_{crit}, and J will be analysed. In addition the influence of the length of the charging time will be studied.

6.2 Influence of hydrogen inflow

The charging rate of hydrogen through the surface is assumed to be $J = 1\times10^{-10}$ kg/m^2/s. Since this parameter cannot be predicted, it has to be verified by checking that the total computed hydrogen content agrees with the experimental values. For the model values presented in the paper this is satisfied. J is the only parameter that is not determined independently of the modelling results.

The experiments presented in the paper are set up in such a way that the hydrogen charging is as large as possible. It can therefore be expected that under other charging conditions, J would be lower. In Figure 6-1 to Figure 6-5 it is illustrated how a change in J would affect the modelling results.

In Figure 6-1 it can be seen that the inflow influences the amount of (atomic) hydrogen in solution in particular at the surface, but the variation there is not quite in proportion to the inflow. At greater depth the amount is fairly independent of the inflow.

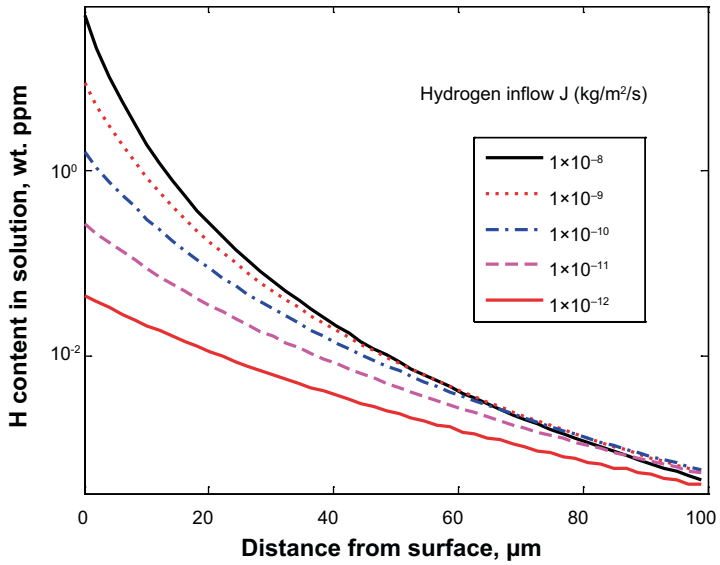

Figure 6-1. *Hydrogen content in solid solution as a function of distance from the surface for five levels of hydrogen inflow at the surface.*

In Figure 6-2 the predicted number of bubbles as a function of distance from the surface is shown. The variation between the inflow levels is largest at the surface.

The bubble diameter versus depth is illustrated in Figure 6-3. Its relative variation with hydrogen inflow is very close to that of the number of bubbles in Figure 6-2. Cut-off for the bubble diameter and the number of bubbles is introduced in Figure 6-2 and Figure 6-3. The reason for the cut-off is described below.

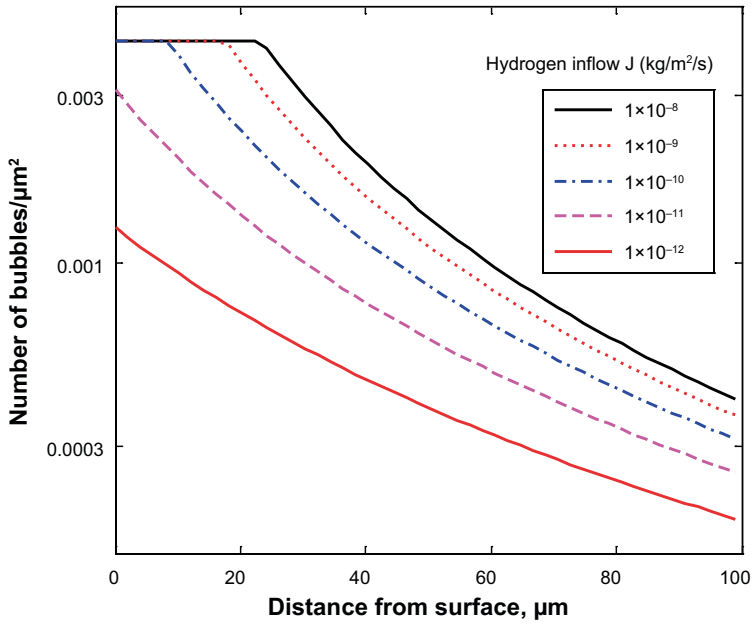

Figure 6-2. *Number of hydrogen bubbles as a function of distance from the surface for five levels of hydrogen inflow at the surface.*

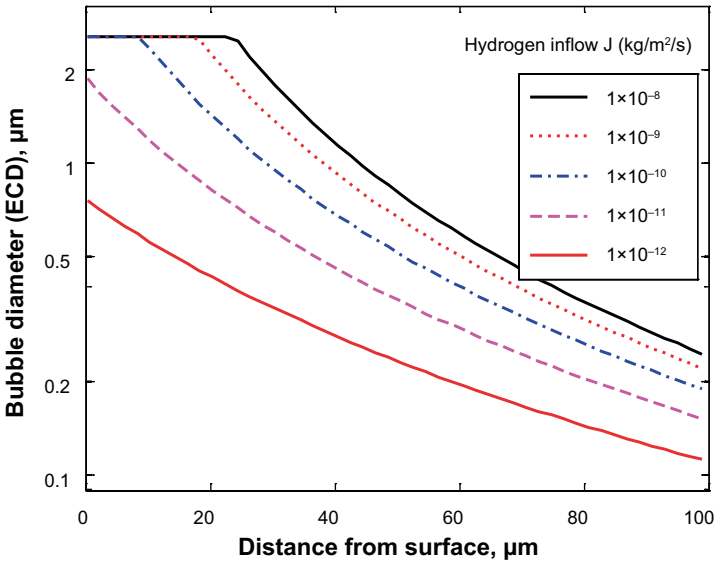

Figure 6-3. *The diameter of bubbles as a function of distance from the surface for five levels of hydrogen inflow at the surface.*

The bubble area fraction f_A can be expressed as

$$f_A = \pi r^2 n_A \qquad \text{Eq (14)}$$

This quantity is illustrated in Figure 6-4. For inflows $\geq 1\times10^{-10}$ kg/m^2/s, the area fraction reaches its maximum value close to the surface. In the paper it was shown that the bubbles become unstable if the distance between them is less than one bubble diameter. With the bubbles in a quadratic net, this gives $f_{Amax} = \pi/16 \sim 0.2$. This value has been used as a cut-off in Figure 6-4.

The density of hydrogen ρ_H (kg/m^3) in a bubble is

$$\rho_H = \frac{p_H}{p_{atm}}\rho_{Hatm} \qquad \text{Eq (15)}$$

where $p_H = 400$ MPa is the hydrogen pressure in the bubbles (Martinsson and Sandström 2012), $p_{atm} = 0.1$ MPa the atmospheric pressure, and $\rho_{Hatm} = 0.0899$ kg/m^3 the hydrogen density at atmospheric pressure. From the hydrogen pressure and the bubble area fraction, the molecular hydrogen content c_{Hmol} can be obtained

$$c_{Hmol} = f_A \frac{\rho_H}{\rho_{Cu}} \qquad \text{Eq (16)}$$

$\rho_{Cu} = 8{,}960$ kg/m^3 is the density of copper. The amount of hydrogen in the material in the form of molecular hydrogen in the bubbles is illustrated in Figure 6-5 using Eq (16). Since the hydrogen pressure in the bubbles is assumed to be constant, Figure 6-5 has precisely the same appearance as in Figure 6-4. The cut-off introduced in Figure 6-4 is also apparent in Figure 6-5. For an inflow of 1×10^{-10} kg/m^2/s, the experimental cut-off is about 2,000 wt. ppm. This indicates that the real cut-off for f_A could be lower but that is not consistent with the observed distribution of bubbles.

The quantity in solid solution is negligible in comparison to the molecular content in the bubbles. The former is at least three orders of magnitude smaller, Figure 6-1. The variation of the amount of molecular hydrogen with inflow is largest at the surface, Figure 6-5. The variation is even somewhat larger than the change in the inflow. Deeper into the material the variation is smaller. This is logical since the total amount integrated over the depth should remain constant.

After three weeks (1.8×10^6 s) with an inflow of 1×10^{-10} kg/m^2/s, the total nominal accumulated amount of hydrogen is 0.00018 kg/m^2. This is the same value 0.00018 kg/m^2 obtained from integrating the content in the bubbles. When the cut-off is taken into account the total amount of hydrogen is reduced for the largest inflows, Table 6-1.

Considering that the real cut-off can be even lower, this might explain why an inflow of 1×10^{-10} kg/m^2/s seems to be close to the maximum possible one experimentally.

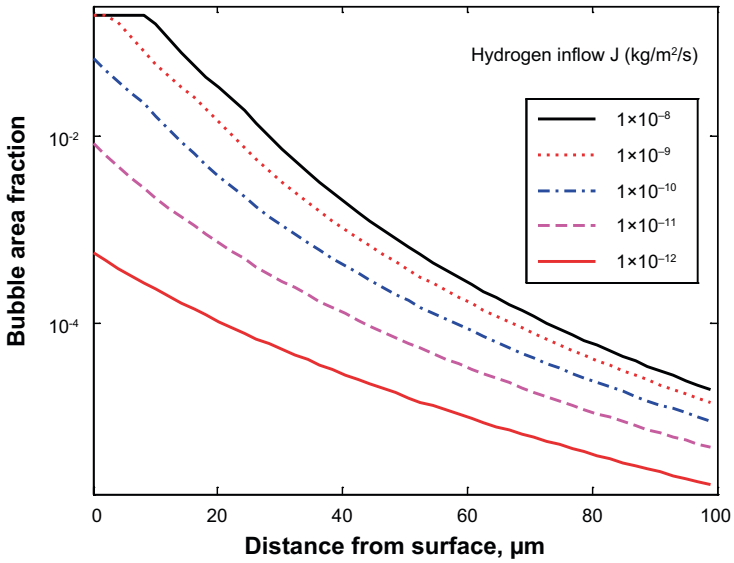

Figure 6-4. *Area fraction of bubbles as a function of distance from the surface for five levels of hydrogen inflow at the surface.*

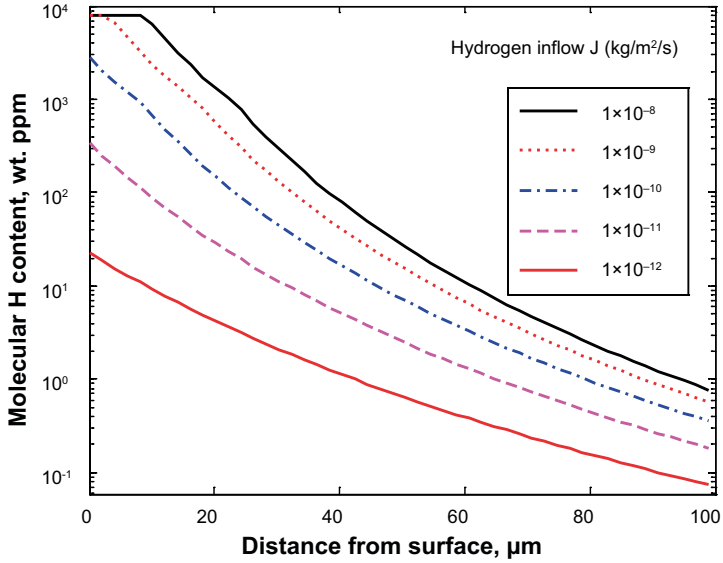

Figure 6-5. *Molecular hydrogen content in bubbles as a function of distance from the surface for five levels of hydrogen inflow at the surface.*

Table 6-1. Total amount of hydrogen.

Inflow of H (kg/m²/s)	1×10^{-8}	1×10^{-9}	1×10^{-10}	1×10^{-11}	1×10^{-12}
Nominal accumulated H content (kg/m²)	0.018	0.0018	0.00018	1.8×10^{-5}	1.8×10^{-6}
Accumulated H content in bubbles with cut-off (kg/m²)	0.0010	0.00064	0.00018	2.4×10^{-5}	2.4×10^{-6}

6.3 Hydrogen charging in foils

In a previous section experimental results for hydrogen charging of foils were presented. The conditions for the charging are identical to those in the paper (Martinsson and Sandström 2012), except for the charging time that is shorter. The chemical solution and the current density are the same. The model summarised above is therefore applicable. The model is compared to the experimental data in Figure 6-6.

In Figure 6-6 a charging time of one week has been assumed in the model. The measured hydrogen content is of the same order of magnitude as the model values. However, the scatter in the experimental results is very high: The amount of scatter is far larger than for the bulk specimen results in Martinsson and Sandström (2012). The reason is that measurements for foils are quite sensitive to the surface condition. Although major efforts have been made to get as clean surfaces as possible, this has obviously not been enough to avoid the influence of the surface conditions.

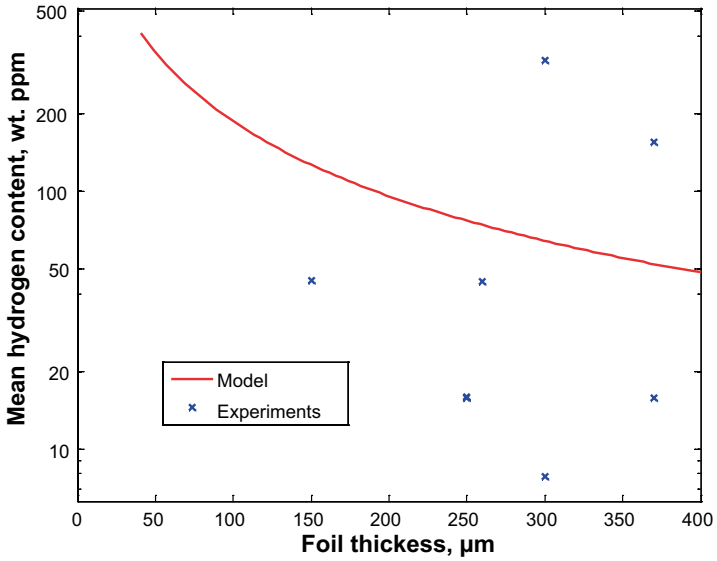

Figure 6-6. *Molecular hydrogen content in foils as a function of foil thickness.*

6.4 Influence of grain size

The grain size plays an important role since most of the hydrogen bubbles are formed at grain boundaries. Possible locations for nucleation of bubbles are grain corners, grain edges, and defects at the boundaries. For simplicity, the grains are assumed to consist of a set of cubes with the side d. Then the number of grain corners per unit volume n_{corn} is

$$n_{\text{corn}} = \frac{1}{d^3} \qquad \text{Eq (17)}$$

The length of grain edges per unit volume L_{edge} is

$$L_{\text{edge}} = \frac{12d}{4d^3} = \frac{3}{d^2} \qquad \text{Eq (18)}$$

This can be seen by considering that each cube has 12 edges and each edge belongs to 4 cubes. Since the critical diameter of a bubble is 2 r_{crit}, cf. Eq (10), the maximum number of nuclei along an edge is $d/(2\,r_{crit})$ and the corresponding number per unit volume is

$$n_{\text{edge}} = \frac{L_{\text{edge}}}{2r_{crit}} = \frac{3}{2r_{\text{crit}}d^2} \qquad \text{Eq (19)}$$

As was shown in the paper, this expression describes well the number of observed bubbles as a function of distance from the surface. This does not mean that all the bubbles are positioned along the grain edges. This would also be impossible since the bubbles are much larger than r_{crit} after growth. Instead many bubbles can be found at defects at the grain sides.

With the help of Eq (11), the expression for n_{edge} (19) can be transferred to the number of bubbles per unit area n_A

$$n_{\text{A}} = \frac{3r}{r_{\text{crit}}d^2} \qquad \text{Eq (20)}$$

This expression for n_A is illustrated in Figure 6-7 as a function of grain size.

Close to the surface the grain size in Eq (20) is directly reflected in the number of bubbles in Figure 6-7. The number of bubbles is proportional to $1/d^2$. Further away from the surface the influence of the grain size is smaller.

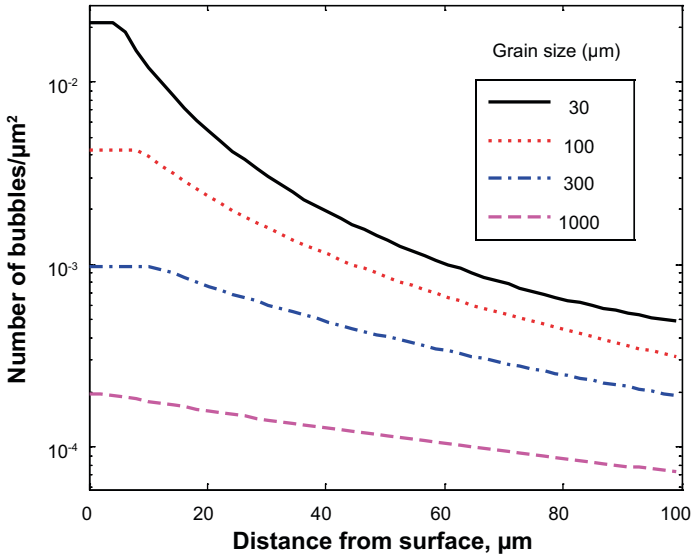

Figure 6-7. *Number of hydrogen bubbles as a function of distance from the surface for four grain sizes.*

In Figure 6-8, the bubble diameter is shown versus distance from the surface. In this case, the largest variation as a function of grain size is inside the material. Close to the surface the both the number of bubbles and their diameter are high in the model, which would give rise to collapse of the bubbles. This can be realised in the following way. From Eq (20) the distance between bubbles in the plane L_A can be obtained.

$$L_A = \frac{1}{\sqrt{n_A}} = \sqrt{\frac{r_{crit} d^2}{3r}} \qquad \text{Eq (21)}$$

This distance must be larger than twice the particle diameter to prevent collapse of the bubbles

$$\frac{L_A}{2r} = \sqrt{\frac{r_{crit} d^2}{3r}} \frac{1}{2r} = \sqrt{\frac{r_{crit} d^2}{12 r^3}} \geq 2$$

which gives

$$r \leq r_{max} = \frac{r_{crit} d^2}{48} \qquad \text{Eq (22)}$$

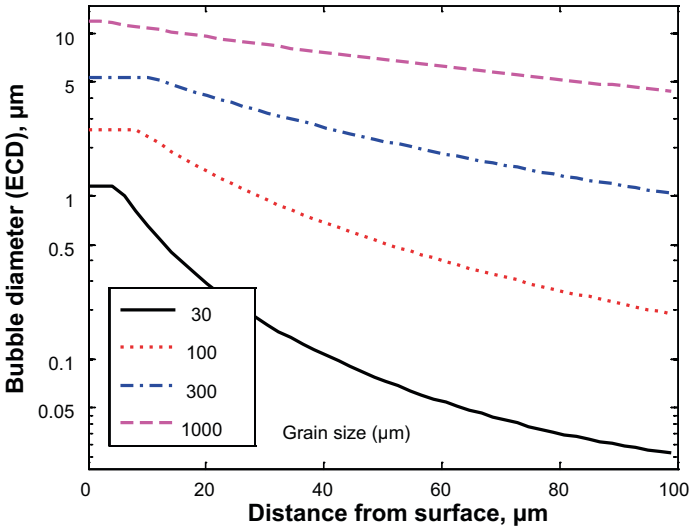

Figure 6-8. *Diameter of hydrogen bubbles as a function of distance from the surface for four grain sizes.*

The maximum bubble diameter according to Eq (22) is taken into account in Figure 6-8 (and in Figure 6-3). If this value is exceeded the bubbles will collapse and form a porous network where the hydrogen will leak out. This is another way of deriving the cut-off in connection with Eq (14).

In Figure 6-9 the resulting bubble area fraction is shown for the four grain sizes. The grain size has a large influence inside the material. For smaller grain sizes the molecular hydrogen is concentrated to the surface area, whereas for the largest grain size significant amount of hydrogen is found 0.1 mm from the surface.

Figure 6-10 illustrates the amount of hydrogen in solid solution. The grain size has quite a direct influence on this quantity. For the largest grain sizes the hydrogen has less opportunity to transfer to the bubbles simply due to the absence of bubble nuclei in the vicinity.

The amount of molecular hydrogen for different grain sizes is shown in Figure 6-11. Since the molecular hydrogen is in the bubbles, Figure 6-9 and Figure 6-11 have precisely the same appearance. By integrating the profiles, the total amount of hydrogen in the material can be obtained. The values found are shown in Table 6-2.

When the grain size is small, the values in Table 6-2 are lower due to the collapse of bubbles close to the surface and the subsequent leakage. In the computations this is a result of the assumed cut-off in Eq (22).

Table 6-2. Total hydrogen content as a function of grain size.

Grain size (µm)	30	100	300	1,000
Accumulated H content in bubbles with cut-off (kg/m^2)	1.2×10^{-4}	1.8×10^{-4}	2.2×10^{-4}	2.0×10^{-4}

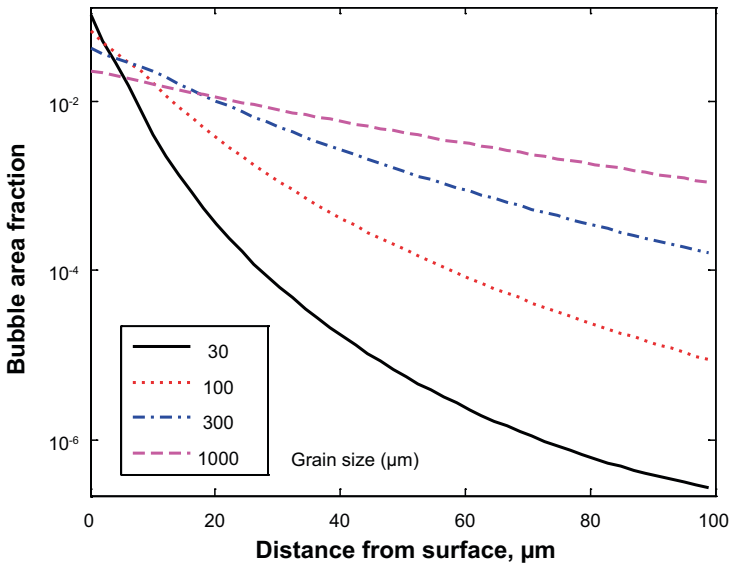

Figure 6-9. *Area fraction of hydrogen bubbles as a function of distance from the surface for four grain sizes.*

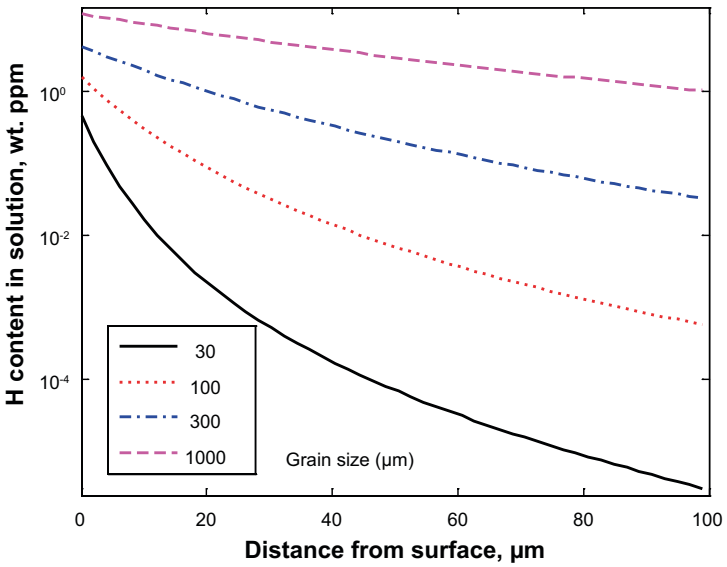

Figure 6-10. *Atomic hydrogen in solid solution as a function of distance from the surface for four grain sizes.*

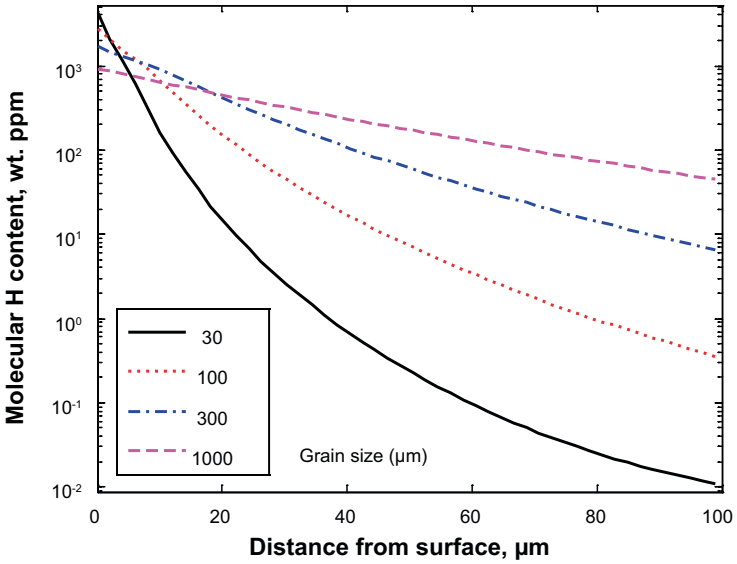

Figure 6-11. *Molecular hydrogen in bubbles as a function of distance from the surface for four grain sizes.*

6.5 Influence of the size of the critical bubble nuclei

The radius r_{crit} of the critical bubble nuclei is given in Eq (10). The value of the pressure p was determined to 400 MPa in the experiments by stress analysis of bubbles close to the surface in the paper. The pressure could be higher inside the material, since each bubble is surrounded by more copper. The pressure range 200 to 800 MPa is considered in the modelling. For the surface energy experimental and theoretical values are found in the interval 1.79 to 2.24 J/m^2 (Vitos et al. 1998). A surface energy of 2.0 J/m^2 is used in the computations. Together with the observed pressure, r_{crit} is equal to 10 nm. An interval between 5 and 20 nm primarily due to the uncertainty in the pressure p should cover possible values for r_{crit}.

The influence of the size of the critical nucleus is illustrated in Figure 6-12. A variation of a factor of three is found at the surface but the variation inside the material is much smaller.

For the bubble diameter the situation is reversed. The variation is largest inside the copper, Figure 6-13.

Since the variation in the diameter is larger than for the number of bubbles, the changes in the diameters dominate the bubble area fraction, Figure 6-14.

For both the hydrogen in solid solution and in the bubbles, the influence of the nucleus size is more pronounced inside the material than at the surface, Figure 6-15 and Figure 6-16.

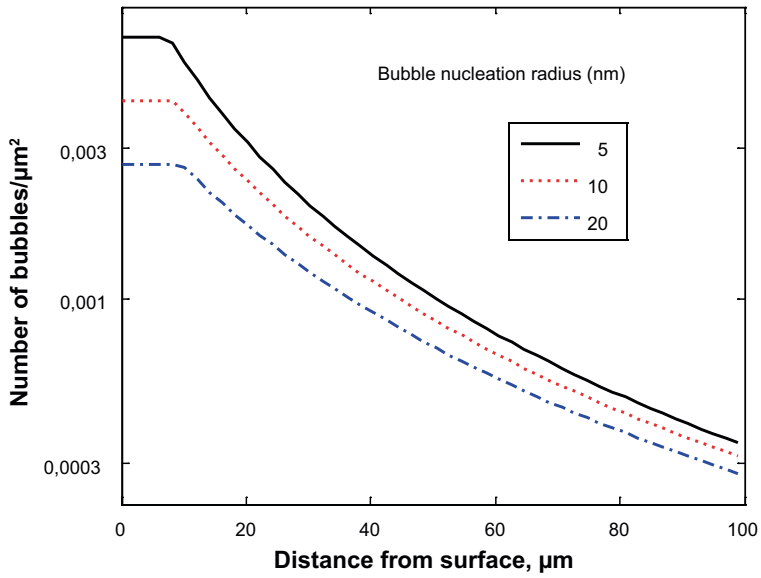

Figure 6-12. *Number of hydrogen bubbles as a function of distance from the surface for three radii of the critical nucleus.*

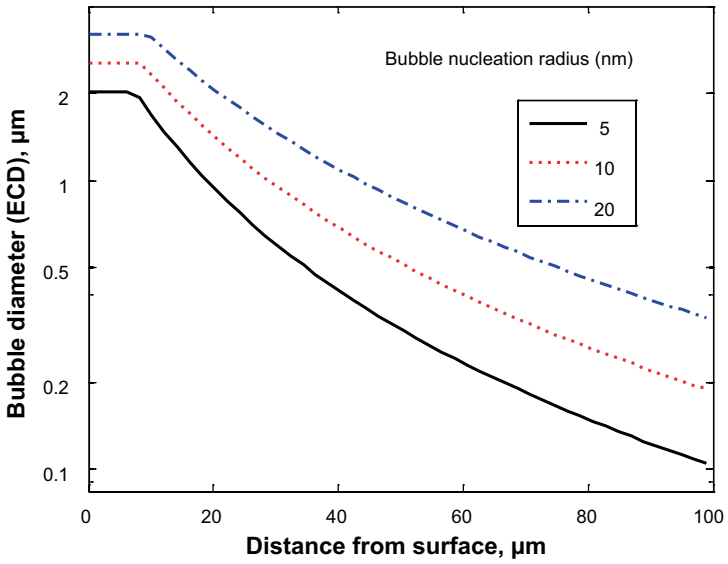

Figure 6-13. *Diameter of hydrogen bubbles as a function of distance from the surface for three radii of the critical nucleus.*

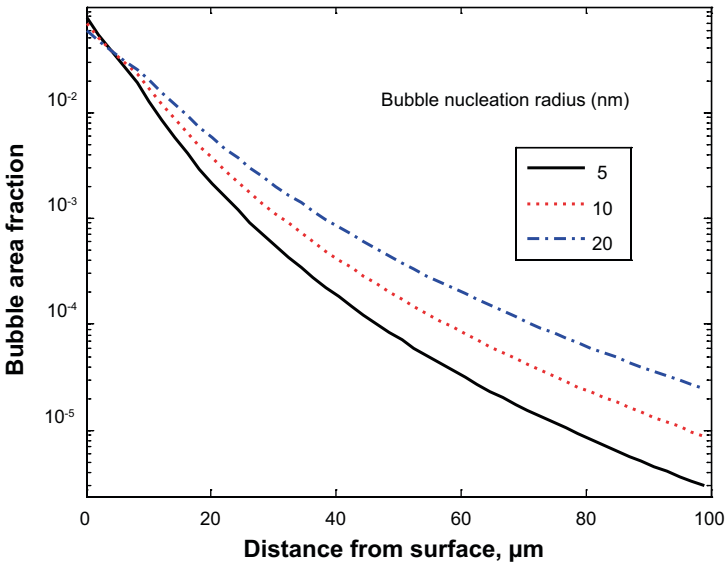

Figure 6-14. *Area fraction of hydrogen bubbles as a function of distance from the surface for three radii of the critical nucleus.*

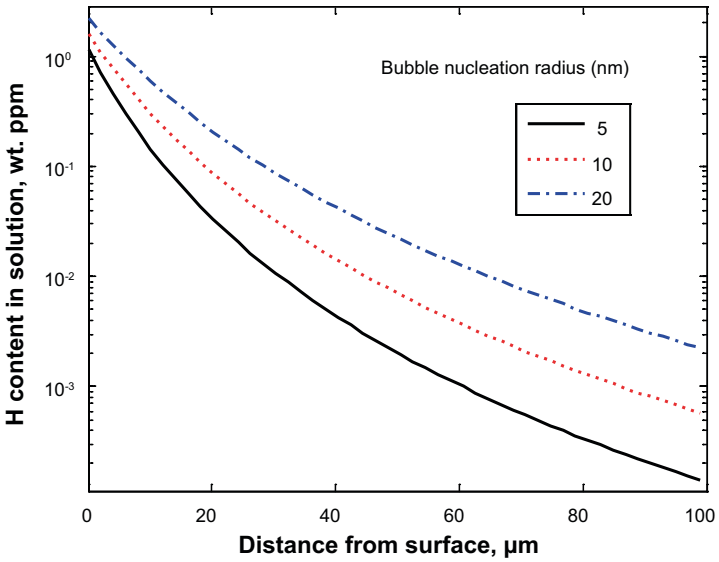

Figure 6-15. *Atomic hydrogen in solid solution as a function of distance from the surface for three radii of the critical nucleus.*

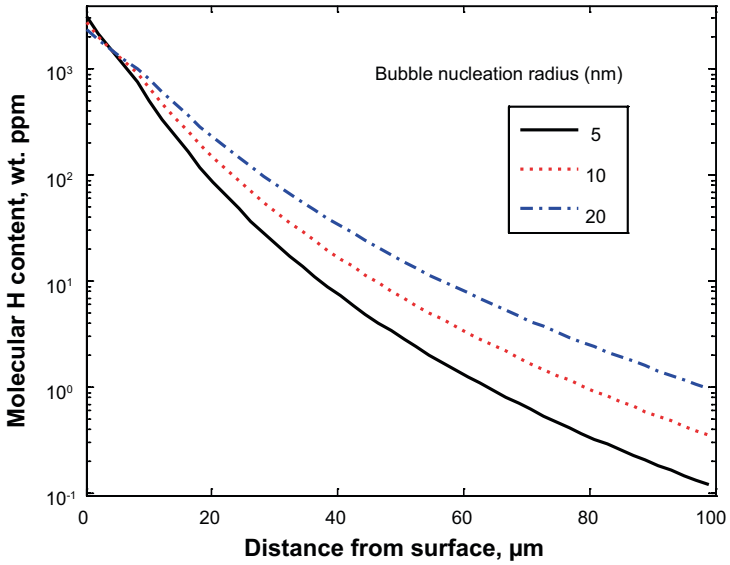

Figure 6-16. *Molecular hydrogen in bubbles as a function of distance from the surface for three radii of the critical nucleus.*

6.6 Influence of charging time

Figure 6-17 illustrates how the amount of hydrogen in solid solution varies with shorter charging times. Initially the amount increases but already after 0.1 weeks a maximum has been reached at a distance of 50 µm or more and then a reduction is observed. The reason is that once the bubbles have reached a certain size the bubbles absorb hydrogen quickly from solid solution.

For longer times there is a rapid decrease, Figure 6-18. This also means that the rate of build up of the total amount of hydrogen is reduced, Figure 6-19.

The bubble diameter and number of bubbles show much the same behaviour, Figure 6-20 and Figure 6-21.

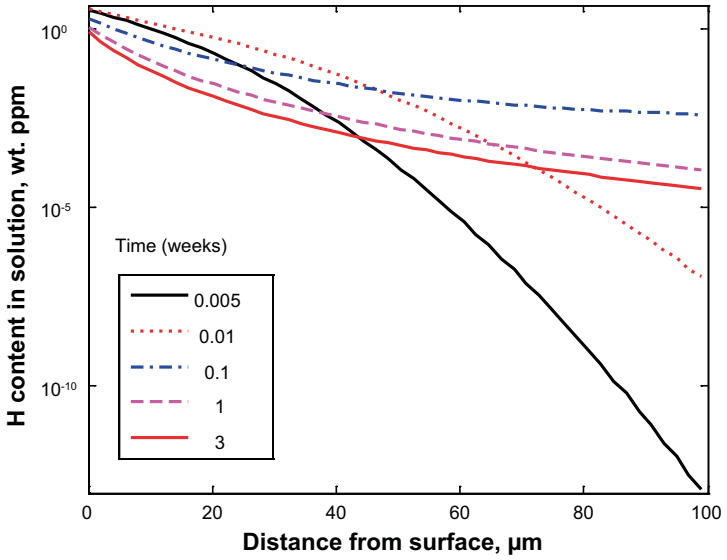

Figure 6-17. *Atomic hydrogen in solid solution as a function of distance from the surface for shorter charging times.*

The rate of increase of the amount of molecular hydrogen is significantly reduced at longer charging times. The reason is the leakage to the surface due to increasing number of larger bubbles there. In addition outflow of atomic hydrogen by general diffusion takes place (Nakahara 1988). This implies that because of the reduced hydrogen built at longer times, a balance between inflow and outflow occurs and a stationary state is reached.

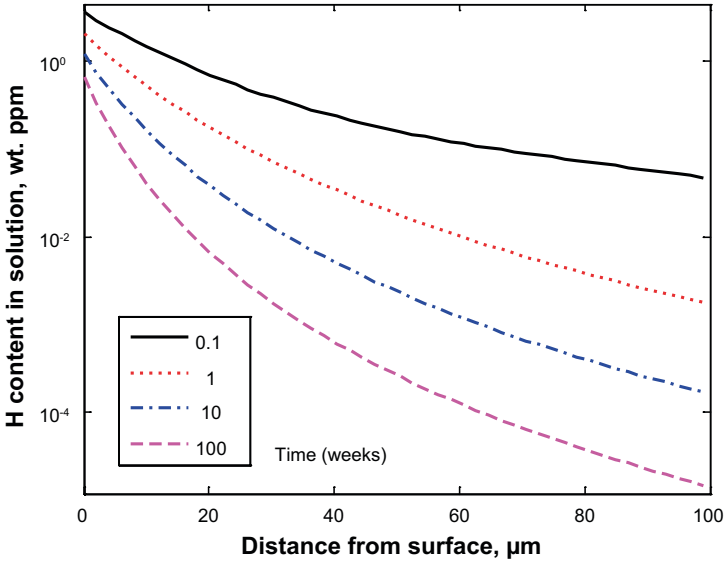

Figure 6-18. *Atomic hydrogen in solid solution as a function of distance from the surface for longer charging times.*

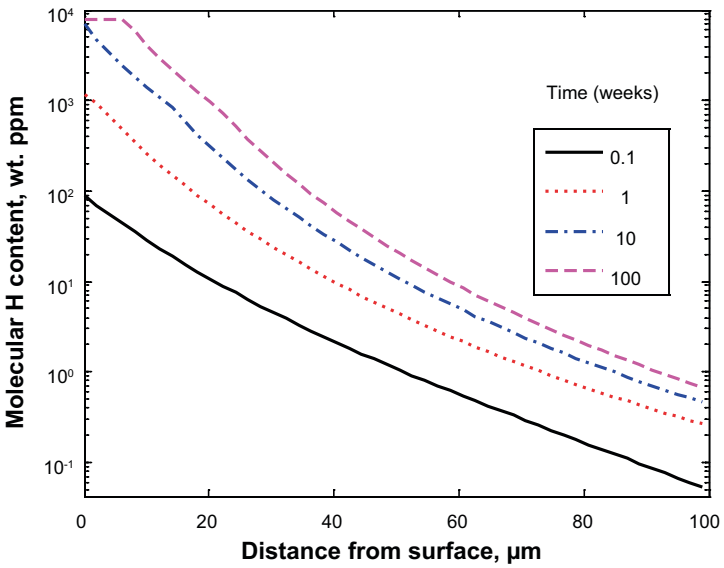

Figure 6-19. *Molecular hydrogen in bubbles as a function of distance from the surface for longer charging times.*

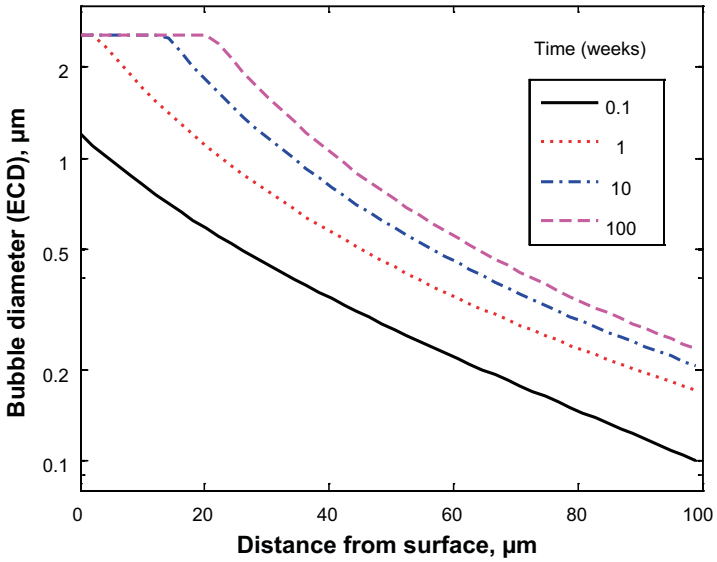

Figure 6-20. *Bubble diameter as a function of distance from the surface for longer charging times.*

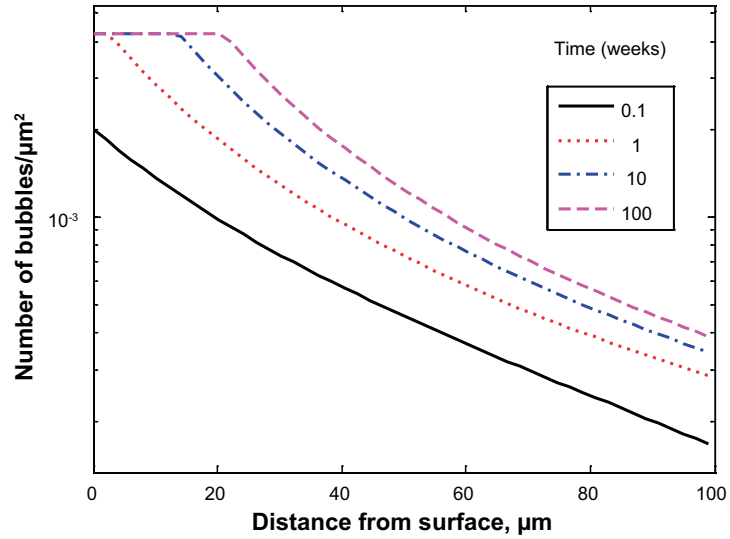

Figure 6-21. *Number of bubbles as a function of distance from the surface for longer charging times.*

7 Conclusions

- The thermal charging method used in this study resulted in a discharging of hydrogen. This is fully consistent with the fact that the solubility of hydrogen is well below 0.6 wt. ppm, which was the amount in the as received materials.
- The electrochemical charging method augmented the hydrogen content from 0.58 to 2.56 wt. ppm in cylindrical bulk specimens.
- The mobility of hydrogen in Cu-OFP is high. After the charging has stopped, it was found experimentally that the amount of molecular hydrogen drops rapidly. Two weeks after electrochemical charging the hydrogen content has been reduced by nearly 40%.
- The method for electrochemical hydrogen charging of foils did not give reliable and reproducible results. In order to determine the solubility of the canister copper and the hydrogen profile after charging, a three-step profile method was later developed.
- A previously published paper (Martinsson and Sandström, 2012) has been used to analyse the hydrogen charging. According to the model the hydrogen is stored in the material in two forms: atomic hydrogen in solid solution and molecular hydrogen in bubbles. During charging the amount of both forms shows an exponential decrease with increasing distance from the surface. The amount of hydrogen is several orders of magnitude higher in the bubbles than in solid solution. With increasing time, the amount in solid solution is reduced quickly by precipitation into the hydrogen bubbles forming molecular hydrogen.
- The experimental results for the foils have been compared to the model. An order of magnitude agreement is obtained. However, the scatter in the observations is very large, most likely due to the difficulty in controlling the surface conditions.
- Parameters in the model were varied to analyse other conditions than in the tests. In particular the inflow of hydrogen, the charging time, the grain size in the copper and the bubble nucleus size were studied.
- The experiments described in this report and in the paper were designed to give maximum charging. That this is closely the case is supported by the developed model. The computed inflow of hydrogen is 1×10^{-10} kg/m^2/s. If a higher inflow is applied in the model the hydrogen bubbles near the surface get so close that they collapse due to the internal pressure. In this way open channels to the surface are formed, where molecular hydrogen can leak out.
- The computations and most of the experiments refer to a charging time of one to three weeks. For longer times the amount of hydrogen in solid solution is rapidly reduced. This means that the build up of the total hydrogen content is slowed down. Consider that an outflow of hydrogen takes place at a rate that is not decreasing. Eventually a stationary state will be reached with a balance between inflow and outflow implying that further built up of the hydrogen content is stopped.
- From published tests on thin foils it is known that high hydrogen contents above 10 wt. ppm can give reduced ductility. From Swedish creep and tensile tests it is well established that copper with 0.6 wt. ppm has fully satisfactory ductility. For the analysed model cases the hydrogen content is below or close to 0.6 wt. ppm, 100 μm into the copper. The only exception is for large grain sizes. For 300 μm grain size the corresponding distance is about 200 μm. For a grain size of 1,000 μm, the 0.6 wt. ppm level is reached at 400 μm distance from the surface. Although this result is not problematic, it is likely that other bubble nuclei inside the grains will become active. This will make the hydrogen profile steeper and shorten the distance to the 0.6 wt. ppm level. Consequently, only a very thin layer of material is exposed to high hydrogen content. The mechanical properties of thick walled components are not influenced in a measureable way. It should also be recalled that in the design premises for the canister a grain size of 360 μm or less is required.

- The critical radius for growth of a bubble depends on the surface energy in the bubble and the hydrogen pressure. The critical radius affects the hydrogen content inside the material but only marginally at the surface.
- In comparison to the charging tests the inflow of hydrogen during corrosion is expected to be less, and the amount of stored hydrogen would be reduced in proportion. The reduction is largest close to the surface.
- If corrosion occurs inside the inserts, hydrogen will form that will enter the cast iron and diffuse inside it. This hydrogen will eventually reach the inner canister wall. The hydrogen could in principle enter the copper through thermal charging, but the temperature is far to low to give a measureable inflow.

Acknowledgement

The authors are grateful to Henrik C. M. Andersson Östling for helpful discussions and review of the manuscript and to Martin Lundholm for performing the hydrogen analyses.

References

SKB's (Svensk Kärnbränslehantering AB) publications can be found at www.skb.se/publications.

Au M, 2003. Mechanical behaviour and fractography of 304 stainless steel with high hydrogen concentration. Report WSRC-TR-2002-00558, Westinghouse Savannah River Company, Aiken, South Carolina.

Caskey G R, Dexter A H, Holzworth M L, Louthan M R, Derrick R G, 1975. Hydrogen transport in copper. Materials Science Symposium of AIME, Cincinnati, Ohio, 11–13 November 1975. Available at: http://sti.srs.gov/fulltext/dpms756/dpms756.pdf

Dayal R K, Parvathavarthini N, 2003. Hydrogen embrittlement in power plant steels. Sādhanā 28, 431–451.

Dull D L, Raymond L, 1974. Electrochemical techniques. In Raymond L (ed). Hydrogen embrittlement testing. American Society for Testing and Materials. (ASTM Special Technical Publication 543), 20–33.

Hoelzel M, Danilkin S A, Ehrenberg H, Toebbens D M, Udovic T J, Fuess H, Wipf H, 2004. Effects of high-pressure hydrogen charging on the structure of austenitic stainless steels. Materials Science and Engineering A 384, 255–261.

Ishikawa T, McLellan R B, 1985. The diffusivity of hydrogen in copper at low temperatures. Journal of Physics and Chemistry of Solids 46, 445–447.

Kennedy J R, Adler P N, Margolin H, 1993. Effect of activity differences on hydrogen migration in dissimilar titanium alloy welds. Metallurgical Transactions A 24, 2763–2771.

Martinsson A, Sandström R, 2012. Hydrogen depth profile in phosphorus-doped, oxygen-free copper after cathodic charging. Journal of Materials Science 47, 6768–6776.

Martinsson Å, Wu R, Sandström R, 2009. Influence of hydrogen on mechanical properties of nodular cast iron. KIMAB-2009-118, Swerea KIMAB AB, Sweden.

McLellan R B, 1973. Solid solutions of hydrogen in gold, silver and copper. Journal of Physics and Chemistry of Solids 34, 1137–1141.

Nagai Y, Saito Y, Matuda N, 1996. Hydrogen desorption from copper during ion bombardment measured by SIMS. Vacuum 47, 737–739.

Nakahara S, 1988. Microscopic mechanism of the hydrogen effect on the ductility of electroless copper. Acta Metallurgica 36, 1669–1681.

Nakahara S, Okinaka Y, 1988. The hydrogen effect in copper. Materials Science and Engineering A 101, 227–230.

Nakahara S, Okinaka Y, 1989. Defects induced in copper by cathodic charging of hydrogen. Journal of The Electrochemical Society 136, 1892–1895.

Nieh T G, Nix W D, 1980. The formation of water vapour bubbles in copper and their effect on intergranular creep fracture. Acta Metallurgia 28, 557–566.

Pan Y, 1986. The positron annihilation study of hydrogen charged copper and copper-aluminium alloys. PhD thesis. The University of Utah. Dissertation abstracts international, Vol. 47-02, Section B, 0683.

Pan Y, Byrne J G, 1985. Thermal charging effects of hydrogen in copper and Cu-Al alloys. Materials Science and Engineering 74, 215–223.

Panagopoulos C N, Zacharopoulos N, 1994. Cathodic hydrogen charging and mechanical properties of copper. Journal of Materials Science 29, 3843–3846.

Pisarek M, Janik-Czachor M, 2006. Microstructural and auger microanalytical characterisation of Cu-Hf and Cu-Ti catalysts. Microscope and Microanalysis 12, 228–237.

Raiko H, Sandstrom R, Rydén H, Johansson M, 2010. Design analysis report for the canister. SKB TR-10-28, Svensk Kärnbränslehantering AB.

SKB, 2006. Kapsel för använt kärnbränsle Konstruktionsförutsättningar. SKB R-06-02, Svensk Kärnbränslehantering AB.

Vitos L, Ruban A V, Skriver H L, Kollár J, 1998. The surface energy of metals. Surface Science 411, 186–202.

Wampler W R, Schober T, Lengeler B, 1976. Precipitation and trapping of hydrogen in copper. Philosophical Magazine 34, 129–141.